ACS Catalysis

pubs.acs.org/acscatalysis

Research Article

Controlled Deposition of Silica on Titania-Silica to Alter the Active Site Surroundings on Epoxidation Catalysts

M. Alexander Ardagh, Daniel T. Bregante, David W. Flaherty, and Justin M. Notestein*

Cite This: *ACS Catal.* 2020, 10, 13008–13018

Read Online

ACCESS | Metrics & More | Article Recommendations | Supporting Information

ABSTRACT: Lewis acidic Ti-SiO_2 materials are workhorse oxidation catalysts, and they range from microporous substituted zeolites to meso/macroporous materials, often with tradeoffs between steric accessibility and activity. In this study, SiO_2 is deposited over the active sites of a macroporous, highly dispersed Ti-SiO_2 catalyst, with or without an organic template. SiO_2 deposition is shown to impact the local environment around epoxidation active sites without altering the active site or introducing diffusion limitations for the representative bulky alkene limonene. Thus, intrinsic activation enthalpies remain nearly constant (45 ± 3 kJ/mol) across all materials and controls, but templated SiO_2 deposition gives an apparent activation enthalpy (9 kJ/mol) much lower than that of the other materials tested because of its strong limonene adsorption. This demonstrates independent control of the active site, its immediate surroundings, and the extended pore structure, while also serving the practical purpose of creating a material that can outperform relevant benchmark materials. These types of materials may find utility in the selective transformation of larger reactants, including biorenewables such as limonene, or precursors for pharmaceuticals and other fine chemicals.

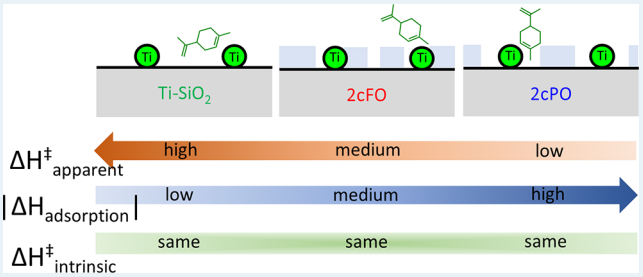

KEYWORDS: *limonene, biorenewables, selectivity, kinetics, oxides*

INTRODUCTION

Supported Lewis acid catalysts have been deployed widely in industrial oxidation processes since the late 1970s. The separate development of Ti-SiO_2 by Shell and zeolite TS-1 by EniChem led to high yield processes for alkene epoxidation and ammoxidation.[1,2] While very effective for propylene and other small reactants, microporous TS-1 is not suited for larger reactants. Subsequently developed mesoporous materials such as Ti-MCM-41 and Ti-SBA-15 have been shown to perform at significantly lower rates than their zeolite analogues in the epoxidation of linear and monocyclic alkenes.[3−5] One interpretation from these studies is that overall epoxidation rates may be highly dependent on the complementarity between reactant alkene size and material pore size. In one set of studies, TS-1 was the most active catalyst for 1-octene, Ti-β was the most active for cyclohexene, and Ti-MCM-41 was the most active for norbornene.[4] However, the overall rate of norbornene epoxidation over Ti-MCM-41 still was far less than that of 1-octene over TS-1. Similarly, Ti-β was more active than Ti-SiO_2 for cyclohexene and styrene epoxidation, which was assigned to stronger reactant adsorption near the active site, a beneficial confinement effect.[6] These confinement effects are also strong functions of the hydrophilicity of the surface in the presence of strongly hydrogen bonding solvents (e.g., water, methanol).[7,8] Those observations motivate this study to use materials synthesis to understand and control local environment effects, independent of the overall pore architecture, in the epoxidation of larger reactants over oxide catalysts.

Limonene, a biomass-derived molecule found in the rinds of citrus fruits, is a terpene with both ring and external double bonds.[9−11] This molecule has promising applications as a precursor to biorenewable thermoplastics such as poly(limonene carbonate). Critical to scaleup of such processes is the selective catalytic production of the ring epoxide (limonene 1,2-epoxide) from limonene.[10,11] Prior studies have shown that a variety of oxide catalysts can epoxidize limonene, but that ring epoxide regioselectivity and epoxidation activity were strongly dependent on reaction conditions, as well as active site sterics and electronics.[12−17] Prior studies have also examined the effect of postsynthetic silylation to alter reaction yields.[18]

Here, we explore the effects of local environment on limonene epoxidation over a class of Ti-SiO_2 catalysts that is synthesized to control the surfaces near the active site without

Received: July 6, 2020
Revised: October 8, 2020

https://dx.doi.org/10.1021/acscatal.0c02937
ACS Catal. 2020, 10, 13008−13018

significantly impacting either the coordination environment at the Ti atom or reactant transport to the active site. Thin layers of SiO_2 are deposited within the pores of a large-pore Ti-SiO_2 catalyst, with and without the presence of an organic template, to alter the surface over and around the grafted Ti active sites. Some of us have used related synthesis techniques to impart size selectivity on a TiO_2 photocatalyst,[19] constrain nanoparticle growth on TiO_2 surfaces,[20] and to create strong Brønsted sites at SiO_2/Al_2O_3 interfaces.[21] Activation barriers and adsorption enthalpies for elementary steps involved in alkene epoxidation have been shown to sense the hydrophobic or hydrophilic nature of the surrounding environment in aqueous oxidants (e.g., H_2O_2 solutions),[7,8] and these barriers also reflect the elemental identity and functional Lewis acid strength of the active sites.[6] To avoid the complicating factors of residual water, protic solvents, and the deactivation that can occur in aqueous H_2O_2 solutions for supported TiOx catalysts, here we compared epoxidation using anhydrous solutions of *tert*-butyl hydroperoxide (TBHP) on microporous zeolite Ti-β and mesoporous Ti-SBA-15 with spectroscopically-similar Ti active sites.

Reaction rates, apparent activation enthalpies, and limonene heats of adsorption are measured to understand the fundamental differences between these catalysts. Although the materials exhibit a wide range of limonene heats of adsorption and apparent epoxidation barriers, the combination of these two factors demonstrates that the catalysts operate via similar intrinsic transition states. When addressing practical considerations surrounding transport effects and the desire to operate at low temperatures, the low apparent activation energy and mesoporous structure result in improved performance for the SiO_2-modified materials as compared to the starting Ti-SiO_2 and a benchmark Ti-β catalyst. These results demonstrate that beneficial effects comparable to zeolite confinement can be introduced by design into large-pore materials that have minimal transport limitations and without changing the structure of the oxidant-activating site. These techniques may be broadly useful in other gas- and liquid-phase reactions, especially for moderately sized, bioderived molecules like terpenes or sugars.

METHODS

Catalyst Synthesis. Ti-SiO_2 was synthesized via the liquid-phase grafting of Cp*$TiCl_3$ ($C_5(CH_3)_5TiCl_3$) onto a mesoporous SiO_2 support that was chosen for its low surface roughness, as evidenced from the low amount of initial microporosity. SiO_2 (Alfa-Aesar, 100−200 mesh, 9 nm pore diameter, ∼375 m^2/g) was dried for 12 h at 190 °C under vacuum to remove physisorbed water. The dry powder was added to a 250 mL round-bottom flask with 50 mL of freshly distilled anhydrous toluene (Sigma-Aldrich, ACS Reagent, ≥99.5%) and a teflon stir bar. An appropriate amount of Cp*$TiCl_3$ (Strem Chemicals, 98%) was added to deposit 0.21 Ti/nm^2 on the support. This mixture was stirred under flowing N_2 at room temperature for 4 h until the dark red color was transferred from the solution onto the solid. Then, the solid was recovered via vacuum filtration on Whatman 42 filter paper, washed with 200 mL toluene and hexanes, and allowed to dry in air. The as-synthesized Cp*Ti-SiO_2 was used directly in subsequent synthetic steps or calcined in static air at 550 °C for 6 h with a 10 °C/min ramp rate to yield Ti-SiO_2 as a bleached white powder.

SiO_2-overcoated variants of Ti-SiO_2 and Cp*Ti-SiO_2 were synthesized using a base-catalyzed sol-gel deposition method. Two grams of Ti-SiO_2 or Cp*Ti-SiO_2 was added to a 500 mL HDPE bottle along with 188 mL of ethanol (Decon Labs, 200 proof, ≥99.9%) and 28 mL of NH_4OH (Macron Fine Chemicals, ACS Reagent, 30%). The powder was dispersed using a sonicator bath for 30 min. Then, 0.65 mL of tetraethylorthosilicate (TEOS, Sigma-Aldrich, ≥99.0%) was added and this mixture was shaken on a gyratory plate at 200 rpm for 1 h. This constitutes the first cycle of SiO_2 overcoating. Subsequent deposition cycles consisted of sonication, TEOS addition, and shaking without the addition of further NH_4OH. Two-cycle and ten-cycle variants were synthesized from Ti-SiO_2 (to give "fully overcoated" 2cFO and 10cFO) and Cp*Ti-SiO_2 (to give "partially overcoated" 2cPO and 10cPO). Upon completion, the powders were recovered via vacuum filtration on Whatman 542 filter paper, washed with 200 mL each of ethanol and hexanes, then allowed to dry in air for 15 min. They were calcined in static air at 550 °C for 6 h with a 10 °C/min ramp rate to yield bleached white powders. The set of overcoated catalysts is described in Supporting Information, Figure S2 along with abridged versions of their synthetic details.

Ti-SBA-15 was synthesized by established co-condensation methods following a prior study.[22] The as-synthesized solid was collected via vacuum filtration on Whatman 542 filter paper, dried in air overnight, and calcined in static air at 550 °C for 6 h with a 10 °C/min ramp rate. Ti-β was synthesized by incorporation of $TiCl_4$ into a dealuminated commercial zeolite β, following a prior study.[6] As for other materials, Ti-β was heated in static air at 550 °C for 6 h with a 10 °C/min ramp rate to yield a bleached white powder before use.

Catalyst Characterization. Surface areas and pore size distributions for all materials were determined using N_2 physisorption at −196 °C on a Micromeritics ASAP 2010 instrument. Prior to N_2 physisorption, all materials were dried under vacuum at 450 °C overnight. The Rouquerol-modified Brunauer−Emmett−Teller (BET) method[23] was used on the adsorption branch of the isotherm to calculate total surface areas and the t-plot (Ti-SiO_2, Ti-SBA-15, Ti-β) or α_S-plot (2cFO, 2cPO, 10cFO, 10cPO) was used to separate out micropore and external surface areas. Mesopore size distributions were obtained from the desorption branch of the isotherm using the BJH method. Ti content for all materials was determined using inductively coupled plasma-optical emission spectrometry (ICP-OES) on a Thermo iCAP 7600 instrument. The samples were prepared by adding HF (Macron Fine Chemicals, 48%, ACS Reagent, CAUTION: store and handle HF with extreme care) dropwise until the sample was dissolved, diluting in 1 vol % aqueous HNO_3 (Fisher Chemical, TraceMetal Grade, 67−70 wt %) solution, and calibrating against diluted solutions of authentic standards, (Sigma-Aldrich, TraceCERT, 1000 mg/L Ti in nitric acid). Edge energies were determined via analysis of the diffuse reflectance UV−vis (DRUV−vis) spectra of the freshly calcined Ti materials and as-made Cp*Ti-SiO_2 based materials. The raw DRUV−vis spectra were smoothed using a 6-point quadratic polynomial Savitzky−Golay filter. Total reflectance was measured under ambient conditions with a Shimadzu UV-3600 Plus UV−vis−NIR spectrophotometer equipped with a Harrick Praying Mantis diffuse reflectance accessory. Polytetrafluoroethylene (PTFE, Sigma-Aldrich, powder, 35 μm particle size) was used as the background for all spectra. Edge

https://dx.doi.org/10.1021/acscatal.0c02937
ACS Catal. 2020, 10, 13008−13018

energies were determined from the x-intercept of the linear portion of the corresponding indirect Tauc plot for each material.

Ti K-edge X-ray absorption near edge structure (XANES) spectroscopy was performed at Sector 5 of the Advanced Photon Source, Argonne National Laboratory, on the DuPont-Northwestern-Dow Collaborative Access Team (DND-CAT) bending magnet D beamline. The beam energy was controlled by a Si(111) monochromator with a resolution of 10^{-4} eV. Incident and transmitted intensities were measured with Canberra ionization chambers. Energies were calibrated in transmission mode against a Ti foil (Sigma-Aldrich), setting the first inflection point at the known edge energy of Ti^0 (4966 eV). Absorption intensities were normalized by their average value between 5050 and 5200 eV in the Athena software package. Known Ti standards Ba_2TiO_4, anatase TiO_2 (Sigma-Aldrich, nanopowder, <25 nm particle size, 99.7% trace metals basis), and fresnoite ($Ba_2(TiO)Si_2O_7$) were brushed onto Kapton tape and their spectra were collected in fluorescence mode. Ti materials were pressed into 30 mg pellets 2.5 cm in diameter and mounted into a 9-pellet controlled atmosphere cell. The pellets were dried in a vacuum oven at 150 °C for 1 h to remove physisorbed water. The vacuum oven was cooled, backfilled with N_2, and the cell was sealed. The spectra were collected in fluorescence mode using a four-channel SII Vortex-ME4 detector. Per prior literature methods,[24,25] the Ti K pre-edge region was fitted to four Gaussian peaks after normalization.

Zero-coverage heats of adsorption of limonene from acetonitrile were measured by van't Hoff analysis within the linear regime of the adsorption isotherm. Full calculation details are found in Supporting Information, Section S4. (R)-(+)-Limonene (Sigma-Aldrich, 97%) was filtered over a column of neutral Al_2O_3 (Fisher Chemical, Brockmann Grade I, 58 Å pore size, 150 m^2/g) immediately before use to remove trace oxygenate contaminants from auto-oxidation. Solutions of limonene in acetonitrile (Fisher Chemical, Optima, ≥99.9%) were heated to a desired temperature between 25 and 55 °C, and an initial sample was taken. ∼30 mg of a Ti material was added to the solution and allowed to equilibrate while shaking at 800 rpm. Two h was found to be adequate to fully equilibrate adsorption. A sample was taken via a Whatman syringe filter (Sigma-Aldrich, 0.7 μm, GF/F). Initial and final samples were analyzed via gas chromatography−mass spectrometry (GC−MS) SIM mode on a Shimadzu GC-MS-QP2010 SE equipped with a Zebron ZB-624 column to determine the initial limonene concentration. The sum of 68, 93, and 67 m/z ion counts was used to quantify limonene concentration and the adsorbed limonene was determined by mass balance. Adsorption isotherms were determined over the range of 5×10^{-6}−10^{-3} M with a linear regime below 3×10^{-5} M.

Measurements of Reaction Kinetics and Selectivities. Limonene epoxidation kinetics were measured in glass vial reactors. For a standard reaction, 25−350 mg of the catalyst was weighed into the reactor, then 4.6 mL of acetonitrile and 0.16 mL of limonene were added. The mixture was shaken at 800 rpm on a heating/cooling stage for 30 min to equilibrate at the desired temperature between 0 and 65 °C. Shaking, rather than stirring, was used to prevent catalysts particles from being sheared. Epoxidation was initiated upon addition of 0.20 mL of *tert*-butyl hydroperoxide (TBHP, Sigma-Aldrich, ∼5.5 M in decane, over molecular sieve 4A). This base case scenario has a limonene concentration of 0.20 M and a TBHP concentration of 0.22 M. To obtain limonene and TBHP reactant orders, their concentration was separately varied from 0.2 to 2.2 M and initial rates were measured. The samples were extracted periodically and syringe-filtered to remove the catalyst. The species were identified by reference to known standards or by GC−MS. The species were quantified using a Shimadzu GC-2010 Plus equipped with an FID and a β-DEX column with calibration factors from authentic standards or their structural isomers. β-DEX is a manufacturer-recommended column for facile separation of terpenes. This chiral column is also able to separate the various enantiomers and diastereomers, should a researcher wish to do so.

For select runs, TBHP concentration was determined by GC−MS SIM mode using decane as an internal standard. Initial rates were extrapolated using data at 15 min or less and correspond to <6% limonene conversion. In all reported data, the carbon balance, as defined by the sum of all products vs consumed reactant, closed to within 95% by quantifying limonene, limonene 1,2-epoxide, limonene 8,9-epoxide, limonene diepoxide, limonene 1,2-diol, limonene 8,9-diol, dihydrocarvone (1,2-saturated limonene 6-one), carveol (limonene 6-ol), carvone (limonene 6-one), peryllil alcohol (limonene 7-ol), and peryllil aldehyde (limonene 7-al). Relevant limonene epoxidation selectivities are defined as follows

$$\textit{epoxide selectivity} = \frac{[\textit{ring epoxide}] + [\textit{external epoxide}]}{[\textit{limonene consumed}]}$$

$$\textit{ring epoxide regioselectivity} = \frac{[\textit{ring epoxide}]}{[\textit{ring epoxide}] + [\textit{external epoxide}]}$$

The standard uncertainty for initial reaction rates was 15% based on run to run variation for triplicate experiments. Kinetic diameters of limonene and titrants were calculated using a limited version of OASIS that is packaged with the publicly available OECD QSAR toolbox. Titration was carried out by phosphonic acid addition to calculate the amount of active TiOx on each catalyst. Phenylphosphonic acid (PPA, Sigma-Aldrich, 98%) or methylphosphonic acid (MPA, Sigma-Aldrich, 98%) was dissolved in mesitylene (Sigma-Aldrich, 98%) or anhydrous 1,2-dimethoxyethane (Sigma-Aldrich, 99.5%, inhibitor-free), respectively, to make 50 mM solutions. Then, 0−0.16 mL of phosphonic acid solution was added to each vial, spanning 0−2 phosphonic acid equivalents per Ti.

RESULTS

Physical and Active Site Characterization. Ti-SiO_2 was synthesized by grafting Cp*$TiCl_3$ ($C_5(CH_3)_5TiCl_3$) under anhydrous conditions onto a large-pore SiO_2 support. The as-synthesized Cp*Ti-SiO_2 was used directly in subsequent synthetic steps or calcined to yield Ti-SiO_2. Other Ti precursors were tested and discarded because they were unstable in the following steps (Supporting Information, Figure S1). SiO_2-overcoated variants were synthesized using repeated cycles of base-catalyzed sol-gel deposition (Scheme 1). Two-cycle and ten-cycle variants were synthesized from Ti-SiO_2 (to give fully overcoated 2cFO and 10cFO) and Cp*Ti-SiO_2 (to give partially overcoated 2cPO and 10cPO). After SiO_2 deposition, the powders were washed, dried, and calcined. Ti-SBA-15 was synthesized by established co-condensation

https://dx.doi.org/10.1021/acscatal.0c02937
ACS Catal. 2020, 10, 13008−13018

Scheme 1. Schematic of Materials Syntheses for Ti-SiO_2, xcFO, and xcPO Materials[a]

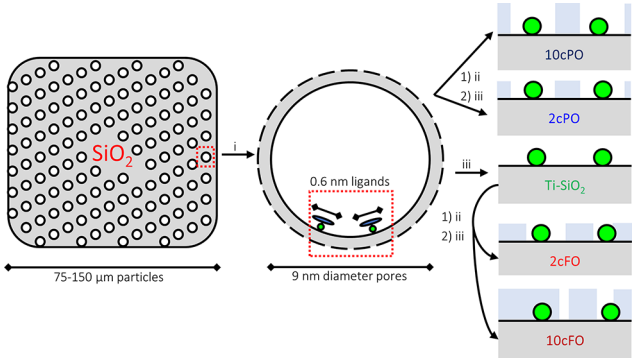

[a](i) Cp*$TiCl_3$ was grafted to large particles of mesoporous SiO_2 from toluene, 4 h, RT. Blue ellipsoid = Cp* ligand approximately 0.6 nm in diameter (ii) 2 or 10 cycles base-catalyzed sol-gel TEOS deposition and (iii) calcination in static air, 550 °C, 6 h. Green circles = deposited TiOx, predominantly as isolated TiOx. Deposited SiO_2 thickness of ∼0.3−1 nm. Note: inconsistent sizes for the sake of clarity in showing active sites and local environments.

methods.[22] Ti-β was synthesized by incorporation of $TiCl_4$ into a dealuminated commercial zeolite β.[6]

A summary of materials characterization data is given in Table 1. N_2 physisorption was first used to assess material pore structure and surface morphology (isotherms in Supporting Information, Figure S2). The SiO_2 support has a wide-pore size distribution centered at 9 nm diameter. Decreases in pore diameter (Figure 1a) indicate that the new SiO_2 layer is ∼0.3 nm thick after 2 deposition cycles (material 2cFO), and it is ∼0.5−1 nm thick after 10 deposition cycles (material 10cFO). The starting SiO_2 initially possessed negligible microporosity, and the deposition cycles introduced small amounts of new microporosity, presumably within the SiO_2 layer, as suggested in Scheme 1. The clear appearance of new microporosity motivates the use of this support, as opposed to a material like SBA-15 that possesses its own microporosity that gets filled in complex ways during grafting steps.[26,27] We were unable to determine the micropore size distribution, and while the size of the templating precursor ligand is ∼0.6 nm, we do not suggest that this directly determines the sizes of the resulting micropores. Ti-SBA-15 has regular mesopores ∼6 nm in diameter.[28] The SiO_2 support is comprised of 75−150 μm aggregates and Ti-SBA-15 is comprised of 4−6 μm aggregates. Ti-β is a crystalline microporous zeolite with a limiting pore diameter of 0.67 nm and the parent β of this sample is comprised of 200 nm aggregates.[29,30]

Ti-SiO_2 was synthesized to have a surface density of 0.21 Ti/nm^2 (0.63 wt % Ti), and the Ti-β and Ti-SBA-15 also have <1 wt % Ti. DRUV−vis spectroscopy (Figure 1b) shows an indirect edge energy of 4.0−4.2 eV for the Ti-SiO_2-based materials, consistent with highly dispersed O_3TiOH.[6,15,31] Ti-SBA-15 has a slightly higher edge energy, and Ti-β a slightly lower edge energy, but both are within the expected range for these materials.[32] None of these have edge energies or shoulders that would indicate the presence of extended domains of TiO_2. In addition, the Ti-SiO_2 spectra are unchanged by the SiO_2 overcoating process, indicating that the coordination geometry at the Ti atoms is largely unchanged.

Ti K-edge XANES measures Ti 3d orbital availability and therefore the average Ti−O coordination number. Figure 2 shows the XANES spectra for experimental catalysts and reference materials for 4-, 5-, and 6-coordinate TiOx (Ba_2TiO_4, fresnoite, and anatase, respectively). The spectra of Ti-SiO_2, 2cPO, 2cFO, 10cPO, and 10cFO are indistinguishable to the eye. The pre-edges were fit to four Gaussians (Supporting Information, Figure S4) following established methods.[24,25] Pre-edge features were sharp for Ti-SiO_2 and the overcoated materials and centered at 4970.1 eV, characteristic of 4-coordinate TiOx. However, their normalized absorption is weaker than that for Ba_2TiO_4, meaning that the active sites are distorted from the perfect tetrahedral configuration. Calibrated against the standard materials, their average coordination numbers (Table 1) are 4.2−4.4, confirming the DRUV−vis assignment as site-isolated, hydroxylated sites. Ti-SBA-15 and Ti-β have similar XANES spectra to Ti-SiO_2 and its modified variants. Considering the speciation results from XANES and DRUV−vis, along with Ti surface densities, these experimental catalysts possess similar, tetrahedral, highly dispersed Ti, which are expected to be active for alkene epoxidation.

Limonene Epoxidation Kinetics over Ti Catalysts. Limonene is a bulky reactant that others have used to probe epoxide selectivity and confinement effects.[3−5,14−16,27,28] Throughout this manuscript, epoxide selectivity refers to the sum of epoxide products relative to limonene consumed.

Table 1. Physical and Active Site Characterization for SiO_2 Supported TiOx Catalysts

	catalyst	Ti loading[a]			edge[b]	CN[c]	active Ti	total SA	micropore SA	pore diameter[f]
ID	name	(mmol/g)	(Ti/nm^2)	(wt %)	(eV)		(%)[d]	(m^2/g)[e]	(m^2/g)[e]	(nm)
	SiO_2							375	nil	9.0
1	Ti-SiO_2	0.13	0.21	0.63	4.0	4.2	103	374	nil	9.0
2	2cFO	0.11	0.21[g]	0.54	4.1	4.3	82	326	37	8.5
3	10cFO	0.07	0.24[g]	0.34	4.1	4.3	35	178	16	8.1
4	2cPO	0.11	0.21[g]	0.54	4.2	4.3	89	324	21	8.3
5	10cPO	0.07	0.24[g]	0.34	4.2	4.4	79	173	40	7.9
6	Ti-SBA-15	0.07	0.05	0.31	4.5	4.5	100	829	331	6.2
7	Ti-β	0.16	0.14	0.77	3.6	4.6	72	683	618	0.67

[a]From Ti ICP-OES and within 5% of expected values from synthesis for Ti-SiO_2-based materials. [b]From DRUV−vis and the *x*-intercepts of indirect transition Tauc plots. [c]Apparent coordination number (CN) from Ti K-edge XANES using the pre-edge peak position and measure of sharpness following deconvolution into Gaussian features.[24,25] [d]From *in situ* titration with MPA during limonene epoxidation at 65 °C. [e]From N_2 physisorption isotherms shown in Supporting Information, Figure S3. [f]From the BJH method applied to the N_2 physisorption desorption branch for all but Ti-β. [g]From the total surface areas after SiO_2 deposition.

https://dx.doi.org/10.1021/acscatal.0c02937
ACS Catal. 2020, 10, 13008−13018

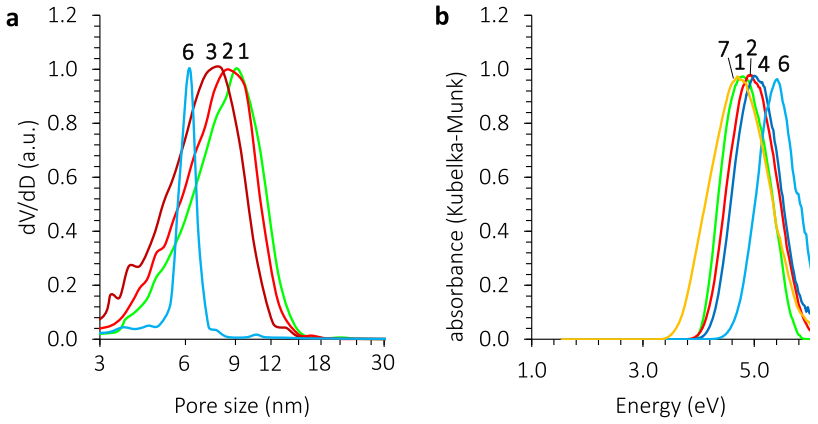

Figure 1. (a) Representative BJH pore size distributions for Ti-SiO_2 (1, green), 2cFO (2, red), 10cFO (3, dark red), and Ti-SBA-15 (6, cyan). Distributions are normalized to their highest peak feature. Remaining distributions can be found in Supporting Information, Figure S3. (b) Representative DRUV−vis spectra of Ti-SiO_2 (1, green), 2cFO (2, red), 2cPO (4, blue), Ti-SBA-15 (6, cyan), and Ti-β (7, orange). 10cFO and 10cPO are indistinguishable from 2cFO and 2cPO, respectively.

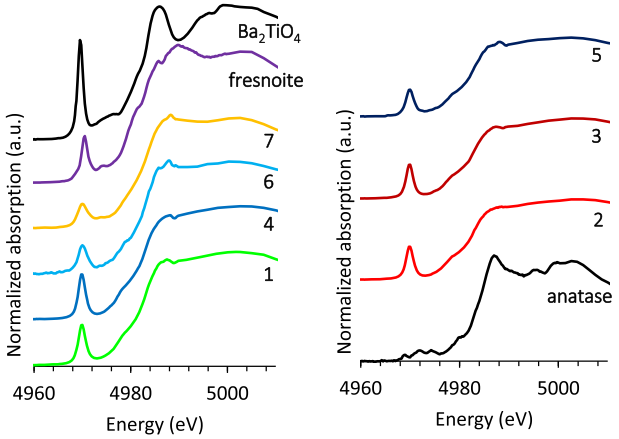

Figure 2. (Left) Ti K-edge XANES for Ti-SiO_2 (1, green), 2cPO (4, blue), Ti-SBA-15 (6, cyan), Ti-β (7, orange), fresnoite (purple), and Ba_2TiO_4 (black). (Right) Ti K-edge XANES for 2cFO (2, red), 10cFO (3, dark red), 10cPO (5, dark blue), and the 6-coordinate TiOx standard anatase. Anatase TiO_2 (black) was obtained from Sigma-Aldrich.

Epoxide regioselectivity refers to the production of the ring epoxide relative to the sum of all epoxide products. When larger pore materials including Ti-β and Ti-MCM-41 were first synthesized, they were tested against benchmark TS-1 (which is minimally active for limonene epoxidation) and Ti-SiO_2 catalysts for limonene epoxidation activity and ring epoxide regioselectivity.[3−5,14−16] Typical regioselectivity values for catalysts such as Ti-SBA-15 and Ti-SiO_2 range from 80 to 90%.[14−16,18,33,34] While other regioselectivity patterns have been observed, this appears to be more a function of reaction conditions (solvent, amount, and type of oxidant) rather than pore morphology. Catalytic performance at 65 °C is shown in Figure 3, expressed as the overall rate of limonene consumption normalized by total Ti content. The normalized rates range from 14 to 60 h^{-1}, which are typical for cycloalkene epoxidation under these conditions.[14−16,22,35] Ring epoxide regioselectivity at 65 °C does not vary between the catalysts, being 85 ± 3 mol %. Product diastereoselectivity was not quantified, but the chromatograms did not noticeably change from sample to sample. SiO_2 exhibits no epoxide production and negligible formation of allylic oxidation products under these conditions. As a negative control not discussed further,

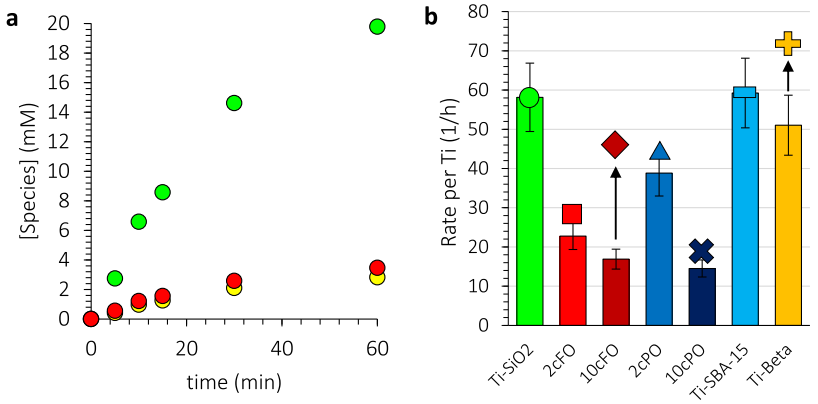

Figure 3. (a) Example concentration vs time plot is shown for Ti-SiO_2 with ring epoxide (green), external epoxide (yellow), and the sum of allylic oxidation products (red). Under these conditions, 10 mM corresponds to 5% yield. Conditions: 65 °C, 30 mg of catalyst (4 μmol Ti), 1 mmol limonene, 1.1 mmol TBHP, 4.6 mL acetonitrile, shaking at 800 rpm. (b) Summary of the initial rates for limonene epoxidation with TBHP in acetonitrile at 65 °C. The bars show the rates normalized per total Ti atom, the symbols show the rates normalized according to the MPA titration results. Ring epoxide regioselectivity is largely invariant between the catalysts; only epoxidation activity is reported here.

https://dx.doi.org/10.1021/acscatal.0c02937
ACS Catal. 2020, 10, 13008−13018

microporous TS-1 (EniChem, 0.53 nm diameter pores) showed negligible epoxide production, consistent with its pores being markedly smaller than the limonene kinetic diameter.

Ti-SiO_2, Ti-SBA-15, and Ti-β have similar initial rates at these conditions, while the rates for the overcoated materials are lower, with Ti-SiO_2 > 2cPO > 2cFO > 10cFO ~ 10cPO. Since differences in epoxidation activity were far greater than differences in ring epoxide regioselectivity, further study was focused on initial activity. We next used Ti site counting by *in situ* phosphonic acid titration[6,22,35] to assess whether these trends in initial rates are due to SiO_2 deposition blocking Ti sites to different extents. Typical titration curves with phenylphosphonic acid (PPA) and methylphosphonic acid (MPA), 0.65 and 0.54 nm kinetic diameter, respectively, are shown in Figure 4 for Ti-SiO_2. For that material, the initial rate

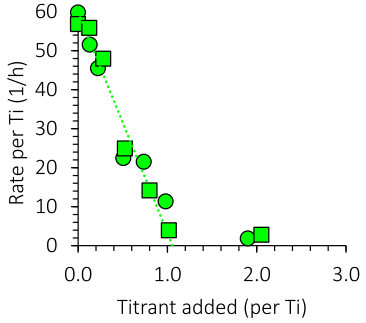

Figure 4. Initial limonene epoxidation rates for Ti-SiO_2 using PPA (□) or MPA (○) added to the reactor during *in situ* titration experiments at 65 °C. The plot uses the initial rates from the first 15 min of reaction.

per metal decreased linearly with added phosphonic acid regardless of the titrant, and the *x*-intercept corresponds to 100 ± 5% active Ti. Ti-SBA-15 has a similarly high active Ti percentage, consistent with the large pores and highly dispersed Ti sites.

In contrast, PPA does not titrate away the activity of Ti-β (Supporting Information, Figure S5), presumably because its kinetic diameter is comparable to the pore dimensions. The smaller MPA titrant gives a linear titration curve and 72% active Ti for Ti-β. This active site count for Ti-β is specific to limonene and TBHP; some of us have demonstrated that 96% of this material's Ti are active for epoxidation of the smaller cyclohexene with H_2O_2.[6] By MPA titration, 2cFO and 10cFO have 82 and 35% active Ti, showing significant site blockage at higher SiO_2 loadings. For this reason, 10cFO was removed from the further study. In contrast, 2cPO and 10cPO were shown to have 89 and 79% active Ti, and the improved site accessibility for these materials, especially relative to the 10cFO variant, demonstrates the positive effect of keeping the Cp* template in place during synthesis. At this point, the rates in Figure 3b can be recomputed per active Ti to give a true turnover frequency (TOF; symbols in Figure 3b). In contrast to our prior studies comparing different grafting precursors on large-pore materials,[22,35] epoxidation TOFs do not converge on a single value here. Therefore, a more detailed investigation was carried out into the materials' kinetics and adsorption behavior.

Limonene Epoxidation Energetics. For all catalysts studied, the rates of limonene consumption at 65 °C increased in proportion to reactant concentration when the limonene concentration was below 1.0 M and when TBHP was below 0.5 M. The rates became insensitive to concentration at higher reactant concentrations. (Supporting Information, Figure S6) Following typical Eley−Rideal mechanisms[36] of olefin epoxidation over Ti-based catalysts,[6,22,37−39] the orders at low concentrations are consistent with a most abundant surface intermediate consisting of a TiOR species, where R might be H, *t*Bu (from co-product *tert*-butanol), or framework Si, depending on the catalyst and extent of reaction. The mechanism then proceeds through reversible binding and activation of TBHP (K_{OOH}) and rate-limiting O transfer to limonene (Lim, k_{ER}). (Scheme 2). Note that in Eley−Rideal mechanisms, limonene does not bind to the active site directly in the kinetically relevant steps.

For the case in Scheme 2, the initial rate is described by eq 1. At negligible product formation (*tert*-butanol, TBOH, and limonene oxide, LO) and low concentrations of the reactants, it simplifies to eq 2, with the observed first-order dependence

Scheme 2. Eley−Rideal Limonene Epoxidation Mechanism[a]

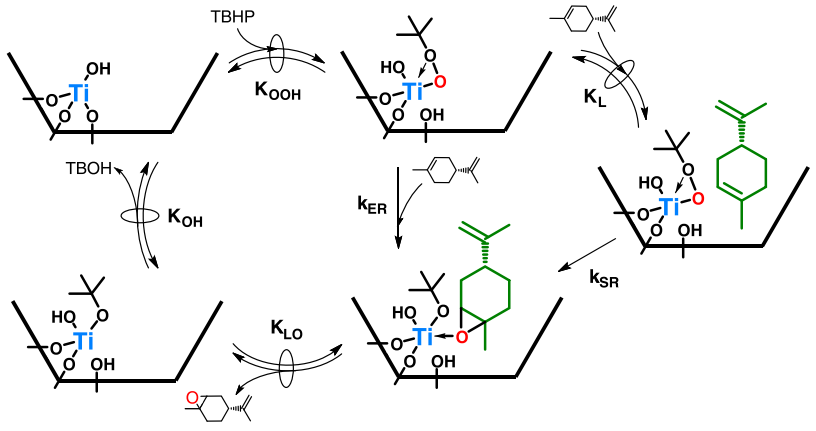

[a]proposed with four elementary steps: quasi-equilibrated adsorption of TBHP, *tert*-butanol (TBOH), and limonene oxide (LO) product, with equilibrium constants K_{OOH}, K_{OH}, and K_{LO}, respectively, as well as rate-limiting, irreversible limonene epoxidation with rate constant k_E. Additional coordinating species, such as acetonitrile solvent, are not drawn for clarity. Rate-limiting step also shown decomposed into two hypothetical steps such that $k_{ER} = k_{SR} \times K_L$.

https://dx.doi.org/10.1021/acscatal.0c02937
ACS Catal. 2020, 10, 13008−13018

on each reactant and a single apparent rate constant, k_{app}. Turnover frequencies (TOF) are based on the count of kinetically relevant Ti atoms determined from MPA titration, above. The cycle shown is for internal H^+ transfer to a Ti−O−Si. Other H^+ transfers could be possible and would alter the value of the enthalpies subsequently determined or add a dependence on water or *tert*-butanol concentration, but would not alter comparisons between the catalysts, as long as we assume that all catalysts operate in the same kinetic regime. The validity of this mechanistic assumption will be borne out if it successfully captures the behavior trends of the set of materials. The geometry drawn for the activated TBHP is intended to be representative only and does not impact the conclusions here.

$$TOF = \frac{rate}{[Ti]_{active}} = \frac{k_{ER}K_{OOH}[TBHP][Lim]}{1 + K_{OOH}[TBHP] + K_{OH}[TBOH] + K_{LO}[LO]} \quad (1)$$

$$TOF_0 = \frac{rate_0}{[Ti]_{active}} = k_{ER}K_{OOH}[TBHP][Lim] = k_{app}[TBHP][Lim] \quad (2)$$

Limonene epoxidation was studied for all catalysts over a range of 35−65 °C. The reaction was first demonstrated to not be limited by mass transfer under these conditions (Supporting Information, Figure S7). The transition-state theory uses the relationship between k_{app} and temperature (eq 3) to calculate apparent enthalpy ($\Delta H_{app}^{\ddagger}$) and apparent entropy ($\Delta S_{app}^{\ddagger}$) of activation.[6,31]

$$k_{app} = \frac{k_B T}{h} K_{app}^{\ddagger} = \frac{k_B T}{h} e^{-\Delta H_{app}^{\ddagger}/RT} e^{\Delta S_{app}^{\ddagger}/R} \quad (3)$$

Eyring plots (Figure 5a) give apparent activation enthalpies ($\Delta H_{app}^{\ddagger}$) ranging from 9 to 34 ± 5 kJ/mol, which is a large range for seemingly similar active site structures (see earlier discussion) operating in the same kinetic regime. Surprisingly, zeolite Ti-β has the highest value, 15 kJ/mol higher than that for Ti-SiO_2 and Ti-SBA-15. This is in contrast with its lower apparent activation enthalpy with reactants like cyclohexene and styrene and with H_2O_2 instead of TBHP.[6] In contrast, SiO_2-overcoated materials 2cFO and 2cPO show a significant decrease in $\Delta H_{app}^{\ddagger}$, 6 and 9 kJ/mol lower than the parent Ti-SiO_2, respectively. Apparent activation entropies ranged from −240 to −165 J/(mol K), which must be due to loss of limonene translational entropy[40] and changes to solvent mobility near the active site.[7,8] Figure 5b shows a strong compensation effect between low apparent activation enthalpies and more negative apparent activation entropies. Lower apparent activation enthalpies reflect stronger adsorption of the reactant, which leads to lower apparent activation entropies, as the reactant loses more degrees of freedom.[40,41] This is illustrated in Figure 5c for Ti-SiO_2 and 2cPO catalysts.

The entropy loss is smallest for Ti-β, which may be a result of the relatively large limonene fitting poorly into these zeolite pores,[42] but also can result from a large entropy gain by released acetonitrile solvent. In contrast, the low apparent activation enthalpies for 2cFO and 2cPO are reminiscent of the behavior seen in transition-state confinement. At this point, we hypothesize that we can remove the compensation effect by

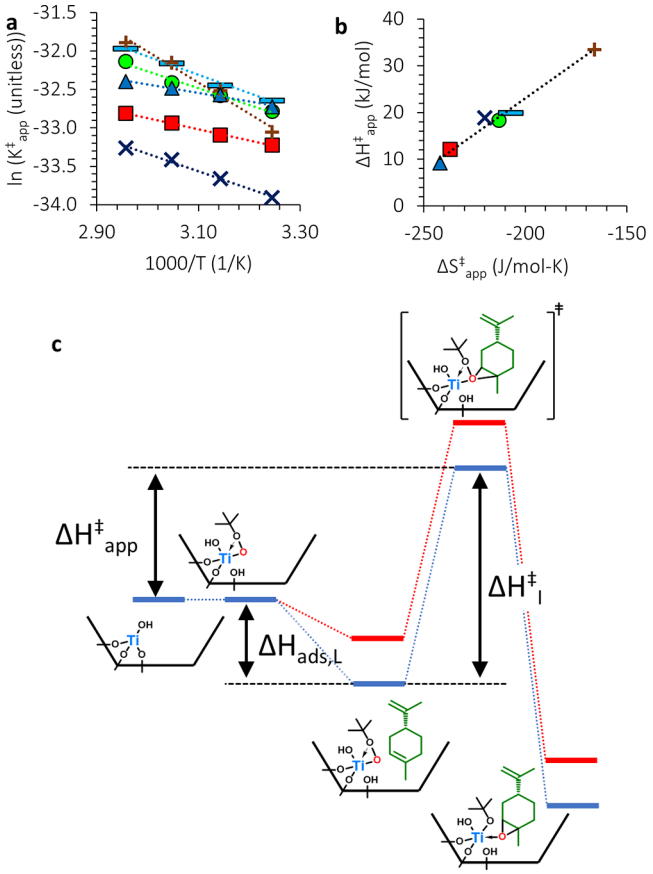

Figure 5. (a) Plot of $\ln(K_{app}^{\ddagger})$ vs $1000/T$ (1/K) for Ti-β (orange, +), Ti-SBA-15 (cyan, −), Ti-SiO_2 (green, ○), 2cPO (blue, Δ), 2cFO (red, □), and 10cPO (dark blue, ×). $K_{app}^{\ddagger}$ as in eq 3. The dashed lines are linear fits to the Eyring equation. Reference concentrations of 1 M were used for both TBHP and limonene in the Eyring equation. (b) Observed compensation between apparent activation enthalpies and entropies obtained from the Eyring plots. (c) Reaction coordinate diagram. Apparent activation enthalpies ($\Delta H_{app}^{\ddagger}$) are treated as the sum of the intrinsic activation enthalpy for epoxidation ($\Delta H_I^{\ddagger} = \Delta H_{SR}^{\ddagger} + \Delta H_{OOH}$) and the heat of adsorption for the limonene reactant ($\Delta H_{ads,L}$) on the SiO_2 surface near the active site. Different materials (e.g., red vs blue curves) are hypothesized to differ primarily in $\Delta H_{ads,L}$.

recasting (Scheme 2, right) the Eley−Rideal rate constant k_{ER} as the product of terms for O transfer alone (k_{SR}) and for physical adsorption of limonene on the SiO_2 surface near the active site (K_L). Equation 4 recollects TBHP activation and O transfer as an "intrinsic" k_I that we hypothesize is dependent only on the electronics of the active Ti atom and not on the unique local environment of each of these catalysts.

$$k_{app} = (k_{ER})K_{OOH} = (k_{SR}K_L)K_{OOH} = (k_{SR}K_{OOH})K_L = k_I K_L \quad (4)$$

Likewise, the apparent enthalpy of activation is given in eq 5 and Figure 5c as the intrinsic enthalpy barrier to activating TBHP and transferring the O atom, $\Delta H_I^{\ddagger}$, and a material-dependent heat of adsorption of limonene, $\Delta H_{ads,L}$. In Figure 5c, ΔH_{OOH} is drawn as ∼0, but any material-independent value will lead to the same conclusions.

$$\Delta H_{app}^{\ddagger} = (\Delta H_{SR}^{\ddagger} + \Delta H_{OOH}) + \Delta H_{ads,L} = \Delta H_I^{\ddagger} + \Delta H_{ads} \quad (5)$$

https://dx.doi.org/10.1021/acscatal.0c02937
ACS Catal. 2020, 10, 13008−13018

Therefore, limonene adsorption experiments were performed to obtain zero-coverage adsorption entropies and enthalpies, from which we can further identify differences in adsorption and intrinsic transition states between the materials. Equilibrium adsorption isotherms (Figure 6) were collected for a representative material set: Ti-SiO_2, 2cFO, 2cPO, Ti-β, and SiO_2, at 40 °C using a literature GC−MS SIM mode analysis that enabled the tracking of limonene concentrations in acetonitrile at values on the order of 10^{-7} M.[43] All isotherms showed adsorption uptake linearly dependent on concentration below 3×10^{-5} M limonene. In some instances, the isotherms extended beyond the linear, Henry regime, in which case Langmuir adsorption isotherms were fit to the experimental data using nonlinear least-squares fitting for K_L (1/M) and the absorption capacity (N_L, mmol/g). Equilibrium adsorption constants were then calculated in the linear regime for all materials between 25 and 55 °C, and the results are shown in Figure 6 and Table 2. The strength of limonene adsorption ($|\Delta H_{ads,L}|$) decreases in the order Ti-SiO_2 > Ti-SBA-15 > Ti-β. The reader is reminded that these are net entropies and enthalpies of adsorption that combine adsorption of limonene on the surface as well as displacement of one or more acetonitrile (solvent) molecules; a large magnitude for the enthalpy of adsorption may reflect the facile displacement of solvent as much as it reflects strong limonene adsorption.

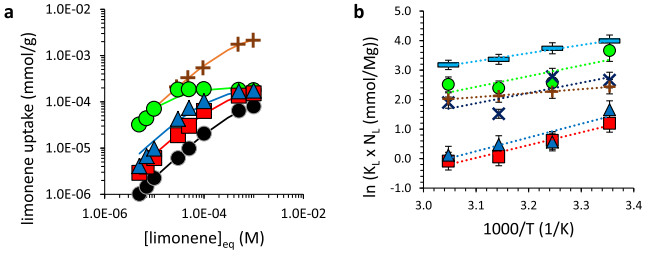

Figure 6. (a) Fitted limonene adsorption isotherms at 40 °C. (b) Relationship between $\ln(K_L \times N_L)$ vs $1000/T$ (1/K) at a limonene concentration of 0.03 mM for Ti-β and 0.007 mM for all others. The dashed lines are least-squares linear regression fits. Ti-SBA-15 (cyan, −), 10cPO (dark blue, ×), Ti-SiO_2 (green, ○), Ti-β (orange, +), 2cPO (blue, Δ), 2cFO (red, □), and SiO_2 (black, ○).

The SiO_2-overcoated materials 2cFO and 2cPO demonstrate significantly stronger limonene adsorption than the conventional materials. 2cFO and 2cPO have 6−9 kJ/mol higher heats of adsorption than their parent Ti-SiO_2. Given that the surfaces of all of these materials are hydroxylated silica, it suggests something akin to steric confinement due to the microporous SiO_2 layer deposited around the active sites. Confinement effects have thus far been exclusively observed for materials with an extended pore structure.[6,41,44] We are unable to directly assess the size of any putative cavity at the active site, and thus we cannot claim a conventional confinement effect. However, these experiments do show that adsorbate stabilization can also arise from the engineering of the local oxide environment.

Finally, since we have defined $\Delta H_{app}^{\ddagger}$ as the sum of $\Delta H_I^{\ddagger}$ and $\Delta H_{ads,L}$, these catalysts should converge on similar $\Delta H_I^{\ddagger}$ if the materials are primarily distinguished by their differences in limonene adsorption. We note that $\Delta H_{ads,L}$ is determined experimentally for limonene on a SiO_2 surface that also possesses bare TiOH sites. This is not necessarily the same as $\Delta H_{ads,L}$ for limonene on a SiO_2 surface that also possesses TiOOR sites, shown in Figure 5c, but we hypothesize that the energetic difference is approximately constant across the set of materials. The validity of this hypothesis will be borne out if $\Delta H_{ads,L}$ is able to explain the differences in catalytic behavior among the materials. The adjusted activation enthalpy values are shown in Table 2, and all six materials tested converge on intrinsic activation enthalpies between 43 and 48 kJ/mol, well within the uncertainty of the adsorption enthalpy measurements. This confirms that SiO_2 deposition enhances limonene adsorption (making $\Delta H_{ads,L}$ more negative) and these enthalpy differences in the catalytic cycle are able to explain the observed differences in the limonene epoxidation rates, as opposed to a change in the intrinsic activation of TBHP and O transfer.

Concerning entropies, the net $\Delta S_{ads,L}$ for limonene on Ti-SiO_2 was near 0, while 2cFO and 2cPO have large negative $\Delta S_{ads,L}$, indicative of less mobile transition state on these surfaces. Once the apparent activation entropies are added to corresponding adsorption entropies, the intrinsic activation entropy also converges on a value of -200 ± 10 J/(mol K). All six materials tested converge on activation enthalpy and entropy values that are indistinguishable within the error of the experiment, strongly suggesting that they all have the same active site. Similarly, this convergence indicates that differences in the rate are due to adsorption of the limonene during the kinetically relevant steps. Regardless of the activity of any specific catalyst or their behavior against any of the benchmark materials, these results demonstrate independent control of the environment surrounding the Ti active site without altering its coordination environment or its intrinsic activity toward activating an oxidant. In the next section, we see that this control can result in practical improvements in catalyst performance.

Impacts for Limonene Epoxidation. The studies shown above support the conclusion that fundamentally, all of the Ti sites in these materials have the same intrinsic activation

Table 2. Summary of Limonene Adsorption and Epoxidation Energetics and Entropies

catalyst	$K_L \times N_L$[a] (mL/g)	$\Delta H_{ads,L}$ (kJ/mol)	$\Delta S_{ads,L}$ (J/(mol K))	$\Delta H_{app}^{\ddagger}$ (kJ/mol)	$\Delta S_{app}^{\ddagger}$ (J/(mol K))	$\Delta H_I^{\ddagger}$[b] (kJ/mol)	$\Delta S_I^{\ddagger}$ (J/(mol K))
Ti-SiO_2	16.0	−30 ± 9	−5.6	18.3	−213	48 ± 9	−207
2cFO	1.53	−36 ± 7	−46.8	12.1	−237	48 ± 7	−190
2cPO	1.98	−39 ± 12	−49.5	9.2	−242	48 ± 12	−193
10cPO	9.04	−29 ± 9	nd[c]	18.9	−220	48 ± 9	nd[c]
Ti-SBA-15	35.0	−23 ± 5	nd[c]	19.9	−207	43 ± 5	nd[c]
Ti-β	9.11	−11 ± 2	28.8	33.5	−166	45 ± 7	−195

[a] $K_L \times N_L$ calculated at 40 °C from a van't Hoff analysis spanning 25−55 °C. [b] Relative errors are much higher for the heat of adsorption values than apparent activation enthalpies due to the nature of the liquid-phase adsorption experiment. [c] N_L was not able to be separately determined for these materials, precluding the calculation of $\Delta S_{ads,L}$ and $\Delta S_I^{\ddagger}$.

https://dx.doi.org/10.1021/acscatal.0c02937
ACS Catal. 2020, 10, 13008−13018

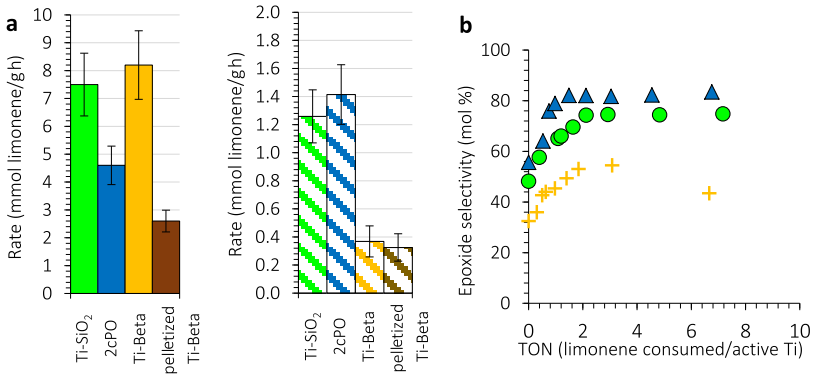

Figure 7. (a) Summary of the initial limonene epoxidation rates with TBHP in acetonitrile at 65 °C (solid) and 0 °C (dashed). Ti-β was pressed into 30 mm pellets, crushed with a mortar and pestle, then sieved to between 100 and 200 mesh particle size. (b) Epoxide selectivity (ring and external epoxides) at 0 °C for Ti-SiO_2 (green, circles), 2cPO (blue, triangles), and Ti-β (orange, plus signs). See Supporting Information, Figure S8 for selectivity at 65 °C.

barrier for epoxidation. Although 2cPO has the lowest apparent activation barrier due to the environment of the deposited SiO_2 layer, the entropic penalty it pays means that, at 65 °C, the observed rate of epoxidation remains higher over Ti-β. However, it should be recalled that these rates were determined for <2 μm crystallites and that any large-scale chemical production, i.e., bioplastics manufacturing, will require the particles to be pressed into much larger aggregates to ease recovery by filtration or to minimize pressure drop through a packed bed.[36,45,46] Moreover, because epoxides are intrinsically unstable, it can be desirable to run reactions at as low a temperature as possible to minimize side reactions that open or eliminate the ring, such as hydrolysis/alcoholysis, oligomerization, and epoxide isomerization. Therefore, Ti-β was pelletized and crushed to 75−150 μm aggregates and compared with high-performing 2cPO and benchmark Ti-SiO_2 catalysts at 0 and 65 °C. The latter catalysts already possess particle sizes in this range.

The catalytic rates for these three catalysts on a per gram basis are shown in Figure 7. When Ti-β is pressed to a larger particle size, its activity decreases by a factor of ~3.2 because internal diffusion limitations become prevalent, and sites in the interior of the particle are exposed to a much lower reactant concentration than those at the external surface.[36,47] This has the result of making the Ti-β sample significantly slower than both Ti-SiO_2 and 2cPO materials, when compared at similar particle sizes. This demonstrates the advantage, from a mass transport perspective, of imparting local effects via oxide deposition around the active sites in a wide-pore environment, rather than via extended microporous structures that can lead to diffusion limitations for larger reactants at industrially relevant particle sizes.

Additionally, it is critical to maintain high epoxide selectivity as conversion increases and to maintain high rates at as low a temperature as possible. Below room temperature, 2cPO is the fastest catalyst because of its much lower apparent activation enthalpy. More importantly, 2cPO maintains ~85% epoxide selectivity at 0 °C, higher than the selectivities of Ti-SiO_2 or Ti-β. Figure 7 plots selectivities against the catalytic turnover number (TON, mol limonene/mol active Ti) to compensate for any differences in catalyst activity. The catalysts Ti-SiO_2 and Ti-β suffer from undesired selectivity to allylic oxidation products that result from radical-mediated processes,[35,47] especially as reaction temperatures decrease. In contrast, the higher epoxide selectivity for 2cPO is directly attributable to its higher limonene heat of adsorption. This conclusively demonstrates that SiO_2 deposition provides a transport limitation-free handle for tunable reactant adsorption that can improve the performance of conventional Ti-SiO_2 materials.

CONCLUSIONS

SiO_2-supported Ti catalysts with diverse structural and surface morphologies were tested in liquid-phase limonene epoxidation to assess the impact of changes to the local environment by silica overcoats on reaction kinetics. SiO_2-overcoated materials 2cPO and 2cFO have the lowest apparent activation enthalpies at 9−12 kJ/mol; 6−9 kJ/mol lower than Ti-SiO_2. Once limonene heats of adsorption were added to corresponding apparent activation enthalpies, the intrinsic $\Delta H_1^{\ddagger}$ to activate THBP and transfer an O converged on 45 ± 3 kJ/mol for all six active materials. From a practical perspective, 2cPO outperforms benchmark catalysts like Ti-β when diffusion limitations are considered, especially in terms of epoxide selectivity at low temperatures. We point out that unlike other surface modifications such as silylation, the 2cPO catalyst remains entirely an oxide and is still chemically Ti-SiO_2. Likewise, these materials might complement conventional approaches to minimizing transport limitations in porous materials (e.g., zeolites) via synthesis of nanoparticles, delaminated materials, or hierarchical zeolites.[45,47−50] This study demonstrates enhanced alkene epoxidation performance via catalyst design used to increase adsorption strength for bulky alkenes, which may have general relevance to a broad class of supported oxide catalysts.

ASSOCIATED CONTENT

Supporting Information

The Supporting Information is available free of charge at https://pubs.acs.org/doi/10.1021/acscatal.0c02937.

Alternate Ti precursors attempted, N_2 physisorption isotherms and additional pore size distributions, XANES pre-edge peak deconvolution example, phosphonic acid titration of Ti-β, rate dependence on limonene and hydroperoxide, particle size test, monoepoxide selectivity, information of the limonene adsorption model (PDF)

https://dx.doi.org/10.1021/acscatal.0c02937
ACS Catal. 2020, 10, 13008−13018

AUTHOR INFORMATION

Corresponding Author

Justin M. Notestein − *Department of Chemical and Biological Engineering, Northwestern University, Evanston, Illinois 60208, United States;* orcid.org/0000-0003-1780-7356; Email: j-notestein@northwestern.edu

Authors

M. Alexander Ardagh − *Department of Chemical and Biological Engineering, Northwestern University, Evanston, Illinois 60208, United States;* orcid.org/0000-0002-0636-8215

Daniel T. Bregante − *Department of Chemical and Biomolecular Engineering, University of Illinois at Urbana-Champaign, Urbana, Illinois 61801, United States;* orcid.org/0000-0003-2157-1286

David W. Flaherty − *Department of Chemical and Biomolecular Engineering, University of Illinois at Urbana-Champaign, Urbana, Illinois 61801, United States;* orcid.org/0000-0002-0567-8481

Complete contact information is available at: https://pubs.acs.org/10.1021/acscatal.0c02937

Notes

The authors declare no competing financial interest.

ACKNOWLEDGMENTS

M.A.A. thanks Louisa Savereide, Scott Nauert, Mihir Bhagat, and Todd Eaton for the helpful discussions and prior syntheses. M.A.A. was supported by the Department of Energy (DOE) through the Institute for Catalysis in Energy Processes (ICEP) and this research was exclusively funded by DOE award # DE-FG02-03-ER154757. D.T.B. and D.W.F. acknowledge support by the U.S. Army Research Office under grant number W911NF-18-1-0100. Metal analysis was performed at the Northwestern University Quantitative Bio-element Imaging Center (QBIC). This research used resources of the Advanced Photon Source, a U.S. Department of Energy (DOE) Office of Science User Facility operated for the DOE Office of Science by the Argonne National Laboratory under Contract No. DE-AC02-06CH11357. M.A.A. thanks Dr. Qing Ma for his seemingly unlimited patience and assistance with the setup for Ti K-edge XANES.

REFERENCES

(1) Wulff, H. P.; Wattimena, F. Olefin Epoxidation. U.S. Patent US4,367,3421977.

(2) Taramasso, M.; Perego, G.; Notari, B. Preparation of Porous Crystalline Synthetic Material Comprised of Silicon and Titanium Oxides. U.S. Patent US4,410,5011983.

(3) Blasco, T.; Corma, A.; Navarro, M. T.; Pariente, J. P. Synthesis, Characterization, and Catalytic Activity of Ti-Mcm-41 Structures. *J. Catal.* **1995**, *156*, 65−74.

(4) van der Waal, J. C.; Rigutto, M. S.; van Bekkum, H. Zeolite Titanium Beta as a Selective Catalyst in the Epoxidation of Bulky Alkenes. *Appl. Catal., A* **1998**, *167*, 331−342.

(5) Wu, P.; Tatsumi, T.; Komatsu, T.; Yashima, T. Postsynthesis, Characterization, and Catalytic Properties in Alkene Epoxidation of Hydrothermally Stable Mesoporous Ti-SBA-15. *Chem. Mater.* **2002**, *14*, 1657−1664.

(6) Bregante, D. T.; Thornburg, N. E.; Notestein, J. M.; Flaherty, D. W. Consequences of Confinement for Alkene Epoxidation with Hydrogen Peroxide on Highly Dispersed Group 4 and 5 Metal Oxide Catalysts. *ACS Catal.* **2018**, *8*, 2995−3010.

(7) Bregante, D. T.; Flaherty, D. W. Impact of Specific Interactions Among Reactive Surface Intermediates and Confined Water on Epoxidation Catalysis and Adsorption in Lewis Acid Zeolites. *ACS Catal.* **2019**, *9*, 10951−10962.

(8) Bregante, D. T.; Johnson, A. M.; Patel, A. Y.; Ayla, E. Z.; Cordon, M. J.; Bukowski, B. C.; Greeley, J.; Gounder, R.; Flaherty, D. W. Cooperative Effects between Hydrophilic Pores and Solvents: Catalytic Consequences of Hydrogen Bonding on Alkene Epoxidation in Zeolites. *J. Am. Chem. Soc.* **2019**, *141*, 7302−7319.

(9) Ciriminna, R.; Lomeli-Rodriguez, M.; Cara, P. D.; Lopez-Sanchez, J. A.; Pagliaro, M. Limonene: a Versatile Chemical of the Bioeconomy. *Chem. Commun.* **2014**, *50*, 15288−15296.

(10) Hauenstein, O.; Agarwal, S.; Greiner, A. Bio-based Polycarbonate as Synthetic Toolbox. *Nat. Commun.* **2016**, *7*, No. 11862.

(11) Hauenstein, O.; Reiter, M.; Agarwal, S.; Rieger, B.; Greiner, A. Bio-Based Polycarbonate from Limonene Oxide and CO_2 with High Molecular Weight, Excellent Thermal Resistance, Hardness and Transparency. *Green Chem.* **2016**, *18*, 760−770.

(12) Mandelli, D.; van Vliet, M. C. A.; Sheldon, R. A.; Schuchardt, U. Alumina-Catalyzed Alkene Epoxidation with Hydrogen Peroxide. *Appl. Catal., A* **2001**, *219*, 209−213.

(13) De P, A. L. V.; Taborda, F.; de Correa, C. M. Kinetics of Limonene Epoxidation by Hydrogen Peroxide on PW-Amberlite. *J. Mol. Catal. A: Chem.* **2002**, *185*, 269−277.

(14) Cagnoli, M. V.; Casuscelli, S. G.; Alvarez, A. M.; Bengoa, J. F.; Gallegos, N. G.; Samaniego, N. M.; Crivello, M. E.; Ghione, G. E.; Perez, C. F.; Herrero, E. R.; Marchetti, S. G. "Clean" Limonene Epoxidation using Ti-MCM-41 Catalyst. *Appl. Catal., A* **2005**, *287*, 227−235.

(15) Gallo, A.; Tiozzo, C.; Psaro, R.; Carniato, F.; Guidotti, M. Niobium Metallocenes Deposited onto Mesoporous Silica via Dry Impregnation as Catalysts for Selective Epoxidation of Alkenes. *J. Catal.* **2013**, *298*, 77−83.

(16) Ivanchikova, I. D.; Skobelev, I. Y.; Maksimchuk, N. V.; Paukshtis, E. A.; Shashkov, M. V.; Kholdeeva, O. A. Toward Understanding the Unusual Reactivity of Mesoporous Niobium Silicates in Epoxidation of C=C Bonds with Hydrogen Peroxide. *J. Catal.* **2017**, *356*, 85−99.

(17) Marino, D.; Gallegos, N. G.; Bengoa, J. F.; Alvarez, A. M.; Cagnoli, M. V.; Casuscelli, S. G.; Herrero, E. R.; Marchetti, S. G. Ti-MCM-41 Catalysts Prepared by Post-Synthesis Methods: Limonene Epoxidation with H_2O_2. *Catal. Today* **2008**, *133*−*135*, 632−638.

(18) Guidotti, M.; Psaro, R.; Batonneau-Gener, I.; Gavrilova, E. Heterogeneous Catalytic Epoxidation: High Limonene Oxide Yields by Surface Silylation of Ti-MCM-41. *Chem. Eng. Technol.* **2011**, *34*, 1924−1927.

(19) Canlas, C. P.; Lu, J. L.; Ray, N. A.; Grosso-Giordano, N. A.; Lee, S.; Elam, J. W.; Winans, R. E.; Van Duyne, R. P.; Stair, P. C.; Notestein, J. M. Shape-Selective Sieving Layers on an Oxide Catalyst Surface. *Nat. Chem.* **2012**, *4*, 1030−1036.

(20) Bo, Z. Y.; Eaton, T. R.; Gallagher, J. R.; Canlas, C. P.; Miller, J. T.; Notestein, J. M. Size-Selective Synthesis and Stabilization of Small Silver Nanoparticles on TiO_2 Partially Masked by SiO_2. *Chem. Mater.* **2015**, *27*, 1269−1277.

(21) Ardagh, M. A.; Bo, Z. Y.; Nauert, S. L.; Notestein, J. M. Depositing SiO_2 on Al_2O_3: a Route to Tunable Bronsted Acid Catalysts. *ACS Catal.* **2016**, *6*, 6156−6164.

(22) Eaton, T. R.; Boston, A. M.; Thompson, A. B.; Gray, K. A.; Notestein, J. M. Counting Active Sites on Titanium Oxide-Silica Catalysts for Hydrogen Peroxide Activation through In Situ Poisoning with Phenylphosphonic Acid. *ChemCatChem* **2014**, *6*, 3215−3222.

(23) Rouquerol, J.; Llewellyn, P.; Rouquerol, F. Is the BET Equation Applicable to Microporous Adsorbents?. In *Studies in Surface Science and Catalysis*; Llewellyn, P. L.; Rodriquez-Reinoso, F.; Rouqerol, J.; Seaton, N., Eds.; Elsevier, 2007; Vol. *160*, pp 49−56.

(24) Farges, F.; Brown, G. E.; Rehr, J. J. Ti K-edge XANES Studies of Ti Coordination and Disorder in Oxide Compounds: Comparison between Theory and Experiment. *Phys. Rev. B* **1997**, *56*, 1809−1819.

(25) Eaton, T. R.; Campos, M. P.; Gray, K. A.; Notestein, J. M. Quantifying Accessible Sites and Reactivity on Titania-Silica (Photo)-Catalysts: Refining TOF Calculations. *J. Catal.* **2014**, *309*, 156−165.
(26) Zukal, A.; Šiklová, H.; Čejka, J. , Grafting of Alumina on SBA-15: Effect of Surface Roughness. *Langmuir* **2008**, *24*, 9837−9842.
(27) Sietsma, J. R. A.; Meeldijk, J. D.; Versluijs-Helder, M.; Broersma, A.; Dillen, A. J. v.; de Jongh, P. E.; de Jong, K. P. Ordered Mesoporous Silica to Study the Preparation of Ni/SiO_2 ex Nitrate Catalysts: Impregnation, Drying, and Thermal Treatments. *Chem. Mater.* **2008**, *20*, 2921−2931.
(28) Kruk, M.; Jaroniec, M.; Ko, C. H.; Ryoo, R. Characterization of the Porous Structure of SBA-15. *Chem. Mater.* **2000**, *12*, 1961−1968.
(29) Chica, A.; Strohmaier, K. G.; Iglesia, E. Effects of Zeolite Structure and Aluminum Content on Thiophene Adsorption, Desorption, and Surface Reactions. *Appl. Catal., B* **2005**, *60*, 223−232.
(30) Dominguez-Dominguez, S.; Berenguer-Murcia, A.; Linares-Solano, A.; Cazorla-Amoros, D. Inorganic Materials as Supports for Palladium Nanoparticles: Application in the Semi-Hydrogenation of Phenylacetylene. *J. Catal.* **2008**, *257*, 87−95.
(31) Thomas, J. M.; Raja, R.; Lewis, D. W. Single-Site Heterogeneous Catalysts. *Angew. Chem., Int. Ed.* **2005**, *44*, 6456−6482.
(32) Tang, B.; Dai, W. L.; Sun, X. M.; Guan, N. J.; Li, L. D.; Hunger, M. A Procedure for the Preparation of Ti-Beta Zeolites for Catalytic Epoxidation with Hydrogen Peroxide. *Green Chem.* **2014**, *16*, 2281−2291.
(33) Charbonneau, L.; Kaliaguine, S. Epoxidation of Limonene over Low Coordination Ti in Ti-SBA-16. *Appl. Catal., A* **2017**, *533*, 1−8.
(34) Guidotti, M.; Ravasio, N.; Psaro, R.; Ferraris, G.; Moretti, G. Epoxidation on Titanium-Containing Silicates: Do Structural Features Really Affect the Catalytic Performance? *J. Catal.* **2003**, *214*, 242−250.
(35) Thornburg, N. E.; Thompson, A. B.; Notestein, J. M. Periodic Trends in Highly Dispersed Groups IV and V Supported Metal Oxide Catalysts for Alkene Epoxidation with H_2O_2. *ACS Catal.* **2015**, *5*, 5077−5088.
(36) Butt, J. B. *Reaction Kinetics and Reactor Design*; Dekker, 2000.
(37) Bonon, A. J.; Kozlov, Y. N.; Bahu, J. O.; Maciel, R.; Mandelli, D.; Shul'pin, G. B. Limonene Epoxidation with H_2O_2 Promoted by Al_2O_3: Kinetic Study, Experimental Design. *J. Catal.* **2014**, *319*, 71−86.
(38) Neurock, M.; Manzer, L. E. Theoretical Insights on the Mechanism of Alkene Epoxidation by H_2O_2 with Titanium Silicalite. *Chem. Commun.* **1996**, *10*, 1133−1134.
(39) Joergensen, K. A. Transition-Metal-Catalyzed Epoxidations. *Chem. Rev.* **1989**, *89*, 431−458.
(40) Van der Mynsbrugge, J.; Janda, A.; Lin, L. C.; Van Speybroeck, V.; Head-Gordon, M.; Bell, A. T. Understanding Brønsted-Acid Catalyzed Monomolecular Reactions of Alkanes in Zeolite Pores by Combining Insights from Experiment and Theory. *ChemPhysChem* **2018**, *19*, 341−358.
(41) Nakamura, K.; Mizuta, R.; Suganuma, S.; Tsuji, E.; Katada, N. Compensation between Activation Entropy and Enthalpy in Reactions of Aromatic Hydrocarbons Catalyzed by Solid Acids. *Catal. Commun.* **2017**, *102*, 103−107.
(42) Sarazen, M. L.; Iglesia, E. Effects of Charge, Size, and Shape of Transition States, Bound Intermediates, and Confining Voids in Reactions of Alkenes on Solid Acids. *ChemCatChem* **2018**, *10*, 4028−4037.
(43) Miller, J. A.; Hakim, I. A.; Thomson, C.; Thompson, P.; Chow, H. H. S. Determination of D-Lmonene in Adipose Tissue by Gas Chromatography-Mass Spectrometry. *J. Chromatogr. B* **2008**, *870*, 68−73.
(44) Chen, J. R.; Li, J. Z.; Wei, Y. X.; Yuan, C. Y.; Li, B.; Xu, S. T.; Zhou, Y.; Wang, J. B.; Zhang, M. Z.; Liu, Z. M. Spatial Confinement Effects of Cage-Type SAPO Molecular Sieves on Product Distribution and Coke Formation in Methanol-to-Olefin Reaction. *Catal. Commun.* **2014**, *46*, 36−40.
(45) Aigner, M.; Grosso-Giordano, N. A.; Okrut, A.; Zones, S.; Katz, A. Epoxidation of 1-Octene under Harsh Tail-End Conditions in a Flow Reactor I: a Comparative Study of Crystalline vs Amorphous catalysts. *React. Chem. Eng.* **2017**, *2*, 842−851.
(46) Russo, V.; Tesser, R.; Santacesaria, E.; Di Serio, M. Chemical and Technical Aspects of Propene Oxide Production via Hydrogen Peroxide (HPPO Process). *Ind. Eng. Chem. Res.* **2013**, *52*, 1168−1178.
(47) Schmidt, I.; Krogh, A.; Wienberg, K.; Carlsson, A.; Brorson, M.; Jacobsen, C. J. H. Catalytic Epoxidation of Alkenes with Hydrogen Peroxide over First Mesoporous Titanium-Containing Zeolite. *Chem. Commun.* **2000**, *21*, 2157−2158.
(48) Burton, A. Recent Trends in the Synthesis of High-Silica Zeolites. *Catal. Rev.* **2018**, *60*, 132−175.
(49) Přech, J.; Pizarro, P.; Serrano, D. P.; Čejka, J. From 3D to 2D Zeolite Catalytic Materials. *Chem. Sci. Rev.* **2018**, *47*, 8263−8306.
(50) Serrano, D. P.; Melero, J. A.; Morales, G.; Iglesias, J.; Pizarro, P. Progress in the Design of Zeolite Catalysts for Biomass Conversion into Biofuels and Bio-Based Chemicals. *Catal. Rev.* **2018**, *60*, 1−70.

https://dx.doi.org/10.1021/acscatal.0c02937
ACS Catal. 2020, 10, 13008−13018